Conjugated Polymer Based Nanoparticles as Dual-Modal Probes for Targeted In Vivo Fluorescence and Magnetic Resonance Imaging

*Kai Li, Dan Ding, Da Huo, Kan-Yi Pu, Ngo Nguyen Phuong Thao, Yong Hu, Zhi Li, and Bin Liu**

A facile strategy is developed to synthesize dual-modal fluorescent-magnetic nanoparticles (NPs) with surface folic acid by co-encapsulation of a far-red/near-infrared (FR/NIR)-emissive conjugated polymer (PFVBT) and lipid-coated iron oxides (IOs) into a mixture of poly(lactic-*co*-glycolic-acid)-poly(ethylene glycol)-folate (PLGA-PEG-FOL) and PLGA. The obtained NPs exhibit superparamagnetic properties and high fluorescence, which indicates that the lipid coated on IOs is effective at separating the conjugated polymer from IOs to minimize fluorescence quenching. These NPs are spherical in shape with an average diameter of ≈180 nm in water, as determined by laser light scattering. In vitro studies reveal that these dual-modal NPs can serve as an effective fluorescent probe to achieve targeted imaging of MCF-7 breast cancer cells without obvious cytotoxicity. In vivo fluorescence and magnetic resonance imaging results suggest that the NPs are able to preferentially accumulate in tumor tissues to allow dual-modal detection of tumors in a living body. This demonstrates the potential of conjugated polymer based dual-modal nanoprobes for versatile in vitro and in vivo applications in future.

1. Introduction

Functional nanoparticles (NPs), which possess functional and structural advantages over discrete molecules and bulk materials, have emerged as a promising class of tools for imaging, cancer diagnosis and drug delivery.[1] As compared to NPs with single modality, dual-modal NPs offer great potentials to satisfy the increasing requirements in advanced biotechnology.[2] In this regard, NPs that combine tumor cell targeting ability with fluorescent and magnetic properties have attracted great interest to benefit in vivo cancer diagnosis and surgical guidance through detection in both modes.[3] Up to now, the fabrication of conventional fluorescent-magnetic NPs has been mainly focused on the combination of organic dyes or quantum dots (QDs) as the optical reagents with iron oxides (IOs) as the magnetic domain.[4] Although QDs are superior to organic dyes in terms of Stokes shift, photostability and emission spectral width,[5] the intrinsic heavy metal components of QDs greatly restrict their application in in vivo diagnosis and therapy.[6] Another problem in these conventional NPs is that the fluorescence of the optical reagents is always sacrificed due to their direct contact with IOs.[7] As a result, it is highly desirable to develop novel fluorescent-magnetic NPs to facilitate in vivo dual-modal imaging.

Fluorescent conjugated polymers are macromolecules with π-conjugated backbones,[8] which have distinguished advantages as compared to small molecule organic dyes in terms of high extinction coefficient and exciton migration.[9] Recently, we and other groups reported various strategies to produce conjugated polymer NPs for cellular imaging studies.[10] These NPs have shown high brightness, good photostability and low cytotoxicity, which make them a promising candidate as the new generation of fluorescence imaging probes.[11] Although initial efforts have been made to prepare fluorescent-magnetic NPs through direct integration of conjugated polymers and IOs, the fluorescence of as-prepared probes is very low,[12] mainly due to the quenching of conjugated polymer fluorescence by IOs. In addition, these NPs have emission wavelengths in the 400–600 nm range, which are not suitable for in vivo imaging. To achieve low autofluorescence and deep tissue penetration for in vivo fluorescence imaging, fluorescent-magnetic NPs with emission in the far-red/near-infrared (FR/NIR) region (650–1000 nm) and large Stokes shift are highly desirable.[13]

In this contribution, we report a one-step strategy to synthesize NPs with cancer cell targeting ability, FR/NIR fluorescence, and superparamagnetic property for in vivo fluorescence

Dr. K. Li, Dr. D. Ding, Dr. K.-Y. Pu,
N. N. P. Thao, Prof. Z. Li, Prof. B. Liu
Department of Chemical and Biomolecular Engineering, National University of Singapore
Singapore 117576
E-mail: cheliub@nus.edu.sg
Dr. K. Li, Prof. B. Liu
Institute of Materials Research and Engineering
3, Research Link, Singapore 117602
D. Huo, Prof. Y. Hu
National Laboratory of Solid State Microstructure
Department of Material Science and Engineering
Nanjing University
Nanjing 210093, P. R. China

DOI: 10.1002/adfm.201102234

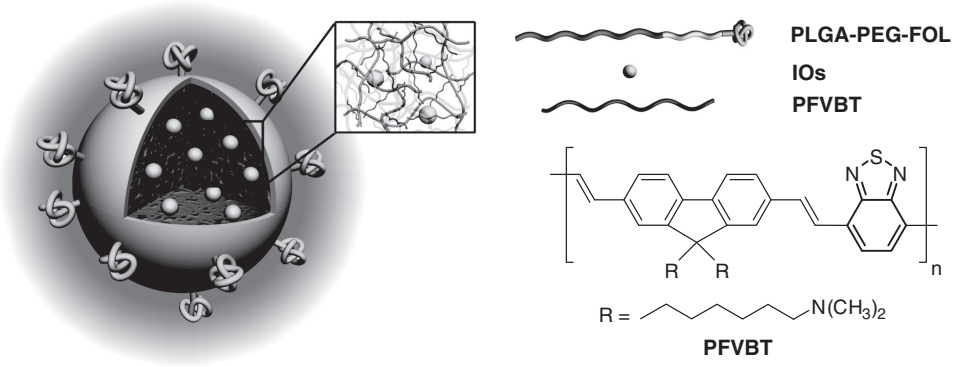

Scheme 1. Illustration of the conjugated polymer based fluorescent-magnetic NP and the chemical structure of PFVBT.

and magnetic resonance imaging applications. The conjugated polymer is designed to show FR/NIR emission by introducing 2,1,3-benzothiadiazole (BT) as the electron deficient unit into a polyfluorenevinylene backbone. IOs are selected as the magnetic domain, and phospholipid is employed for IOs coating to separate them from conjugated polymers to minimize fluorescence quenching. A mixture of poly(lactic-*co*-glycolic-acid)-poly(ethylene glycol)-folate (PLGA-PEG-FOL) and PLGA is used as the encapsulation matrix to yield fluorescent-magnetic NPs born with surface folic acid groups. The targeting ability of the obtained dual-modal NPs to folate receptor-overexpressed cancer cells as well as their in vivo fluorescence imaging and magnetic resonance imaging (MRI) are investigated.

2. Results and Discussion

2.1. Synthesis and Characterization of Dual-Modal NPs

Poly[9,9-bis(6′-(*N*,*N*-dimethylamino)hexyl)fluorenyldivinylene-*alt*-4,7-(2,1,3,-benzothiadiazole)] (PFVBT) was designed and synthesized as the fluorescent polymer for NP formation.[14] Oleic acid coated IOs (OA-IOs) with superparamagnetic property were synthesized according to literature.[15] The high resolution transmission electron microscopy (HR-TEM) image of OA-IOs is shown in Figure S1 in the Supporting Information. The OA-IOs were subsequently treated with a phospholipid of 2-distearoyl-*sn*-glycero-3-phosphoethanolamine (DSPE) to yield DSPE coated IOs (DSPE-IOs) that are soluble in various organic solvents. To investigate the influence of IOs surface coating on the optical properties of fluorescent-magnetic probes, OA-IOs or DSPE-IOs (1 mg of IOs for both) and PFVBT (1 mg) were encapsulated into a mixture of PLGA and PLGA-PEG-FOL (molar ratio 9:1) to yield two batches of NPs.[16] The fluorescence intensity of PFVBT NPs co-encapsulated with OA-IOs is about 55% of that with DSPE-IOs (Figure S2 in the Supporting Information). In addition, the fluorescence for PFVBT/DSPE-IOs is only slightly lower (<5%) than that for the pure PFVBT NPs, and the difference is largely due to the light absorption of IOs. Considering that both NPs share the similar loading efficiencies of OA-IOs and DSPE-IOs (Table S1 in the Supporting Information), the results suggest that DSPE can act as an efficient barrier to reduce the contact between PFVBT and IOs to avoid fluorescence quenching. The generality of this strategy to fabricate dual-modal imaging probes without sacrificing the fluorescent property is further confirmed with other conjugated polymers as described in the Supporting Information.

To facilitate targeted in vivo fluorescence and magnetic resonance imaging, surface folic acid functionalized NPs (FMCPNPs) were prepared by encapsulating PFVBT (1 mg) and DSPE-IOs (4 mg of IOs) using a mixture of PLGA and PLGA-PEG-FOL (feed molar ratio 9:1) through nanoprecipitation method. The structural illustration of the obtained NPs is shown in **Scheme 1**. The encapsulation efficiency of PFVBT is 45% by comparing the fluorescence intensity of the freeze-dried NPs dissolved in THF to that of a calibration curve. Inductively coupled plasma mass spectrometry (ICP-MS) study reveals that 49% of the DSPE-IOs are encapsulated. The UV-vis absorption and photoluminescence (PL) spectra of FMCPNPs in aqueous suspension are shown in **Figure 1**a. The absorption and emission maxima for FMCPNPs are at 516 and 636 nm, respectively. The intense emission tail in the PL spectrum after 700 nm suggests that these NPs hold great potential for in vivo FR/NIR imaging. The magnetic property of FMCPNPs was evaluated using vibrating sample magnetometer (VSM) as shown in Figure 1b. FMCPNPs exhibit superparamagnetic behavior at 298 K with a saturated magnetization value of 3.42 emu/g, which is sufficient for in vivo magnetic resonance imaging.

Laser light scattering (LLS) results indicate that FMCPNPs have a volume average hydrodynamic diameter of 176 ± 3 nm. The size distribution of FMCPNPs is shown in **Figure 2**a. The morphology of the as-prepared FMCPNPs was investigated by field emission scanning electron microscopy (FESEM) and HR-TEM, which are shown in Figure 2b,c, respectively. The FESEM image reveals that FMCPNPs have spherical shape with smooth surfaces. The HR-TEM image in Figure 2c shows that the DSPE-IOs (dark dots) are randomly embedded in polymeric NPs (gray). This is further confirmed by X-ray photoelectron spectroscopy (XPS) result, which provides the chemical composition of particle surface (Figure S3 in the Supporting Information). There is no characteristic peak of iron element at 686 eV, suggesting that the IOs are encapsulated inside NPs rather than adsorbed on surface. In addition, the peak at 397.6 eV in

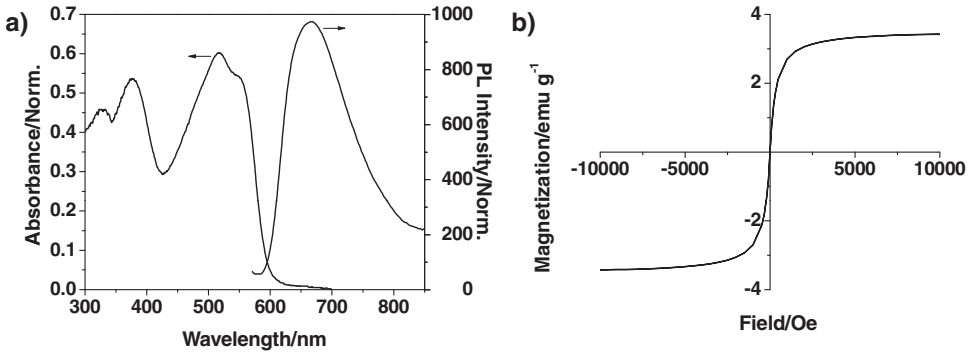

Figure 1. a) UV-vis absorption and PL spectra of FMCPNPs aqueous suspension (λ_{ex} = 518 nm). b) Hysteresis curve of FMCPNPs.

the XPS spectrum of FMCPNPs indicates the presence of folic acid on the NP surface.

2.2. Targeted Cancer Cell Imaging

The targeting ability of FMCPNPs to folate receptor-overexpressed cancer cells was studied using MCF-7 breast cancer cells as an example.[17] As a control group, PFVBT and DSPE-IOs loaded NPs without surface folic acid (MCPNPs) were also prepared using pure PLGA as the encapsulation matrix. The obtained NPs have shown similar physical and optical properties to those of FMCPNPs (Table S2 in the Supporting Information). **Figure 3**a,b show the confocal images of MCF-7 breast cancer cells after incubation with MCPNP and FMCPNP suspensions for 4 h in culture medium at 0.25 mg/mL of NPs, respectively. The cell nuclei were stained with 4',6-diamidino-2-phenylindole (DAPI). These images were taken upon excitation at 488 nm (2.5 mW laser power) with a 650 nm longpass barrier filter. The higher fluorescence intensity observed in Figure 3b as compared to that in Figure 3a indicates that more FMCPNPs are internalized into MCF-7 cells via folate receptor-mediated endocytosis.[10c] This is confirmed by the study of competitive effect of free folic acid on the endocytosis of FMCPNPs. The fluorescence image of free folic acid-pretreated MCF-7 cancer cells after incubation with 0.25 mg/mL of FMCPNPs is shown in Figure 3c. The lower fluorescence intensity from NPs in Figure 3c as compared to that in Figure 3b reveals that the uptake of FMCPNPs is greatly inhibited by free folic acid treatment, which effectively blocks the interaction between FMCPNPs and the folate receptors on cell surface.[18]

Quantitative analysis using Imaging-Pro Plus software suggests that the average red fluorescence intensity in Figure 3b is ~1.4 and 1.3 times brighter as compared to those in Figure 3a,c. 3D confocal image of cells incubated with FMCPNPs shows that the intense fluorescence is mainly from NPs internalized into the cell cytoplasm (Figure 3d). It is noteworthy that no autofluorescence from the cell itself can be detected under the same experimental condition (Figure 3e). The cellular uptake was also quantitatively investigated by flow cytometry. The flow cytometry histograms of MCF-7 cancer cells after incubation with FMCPNPs and MCPNPs (0.25 mg/mL of NPs) for 4 h at 37 °C are shown in Figure 3f. The average fluorescence intensity of each cell incubated with FMCPNPs is ~1.4 times higher as compared to that upon incubation with MCPNPs. It should be noted that more than 99% of the cells are effectively stained by the NPs to show intense fluorescence as compared to the control cells without incubation with NPs. The same gate is used to determine the mean fluorescence for each sample as shown in the SSC/FSC in Figure S4 in the Supporting Information.

As a critical issue in bioimaging, the cytotoxicity of FMCPNPs was evaluated by the metabolic viability of both MCF-7 cancer cells and NIH/3T3 fibroblast cells using methylthiazolyldiphenyl-tetrazolium (MTT) assay. **Figure 4** summarizes the metabolic viability of the MCF-7 and NIH/3T3 cells after incubation with FMCPNPs at 1, 2, and 3 mg/mL of NPs for 48 and

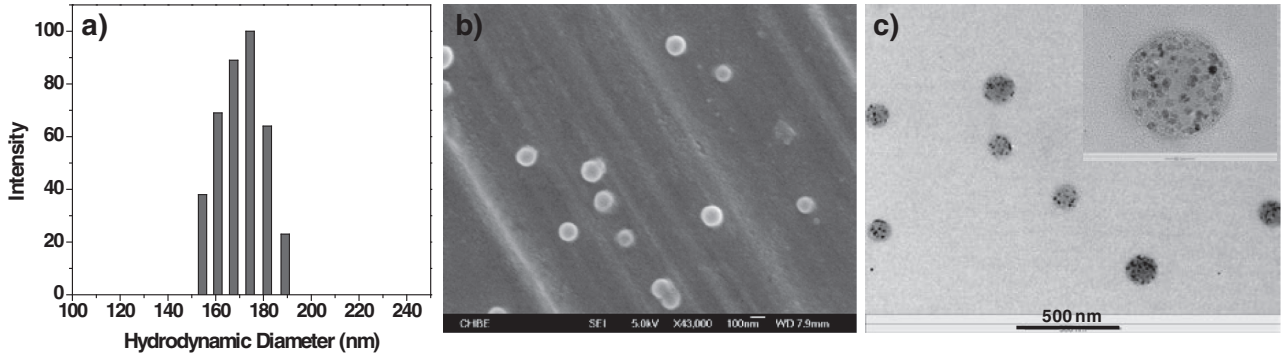

Figure 2. a) Size distribution of FMCPNPs in water studied via laser light scattering. b) FESEM and c) HR-TEM images of the FMCPNPs.

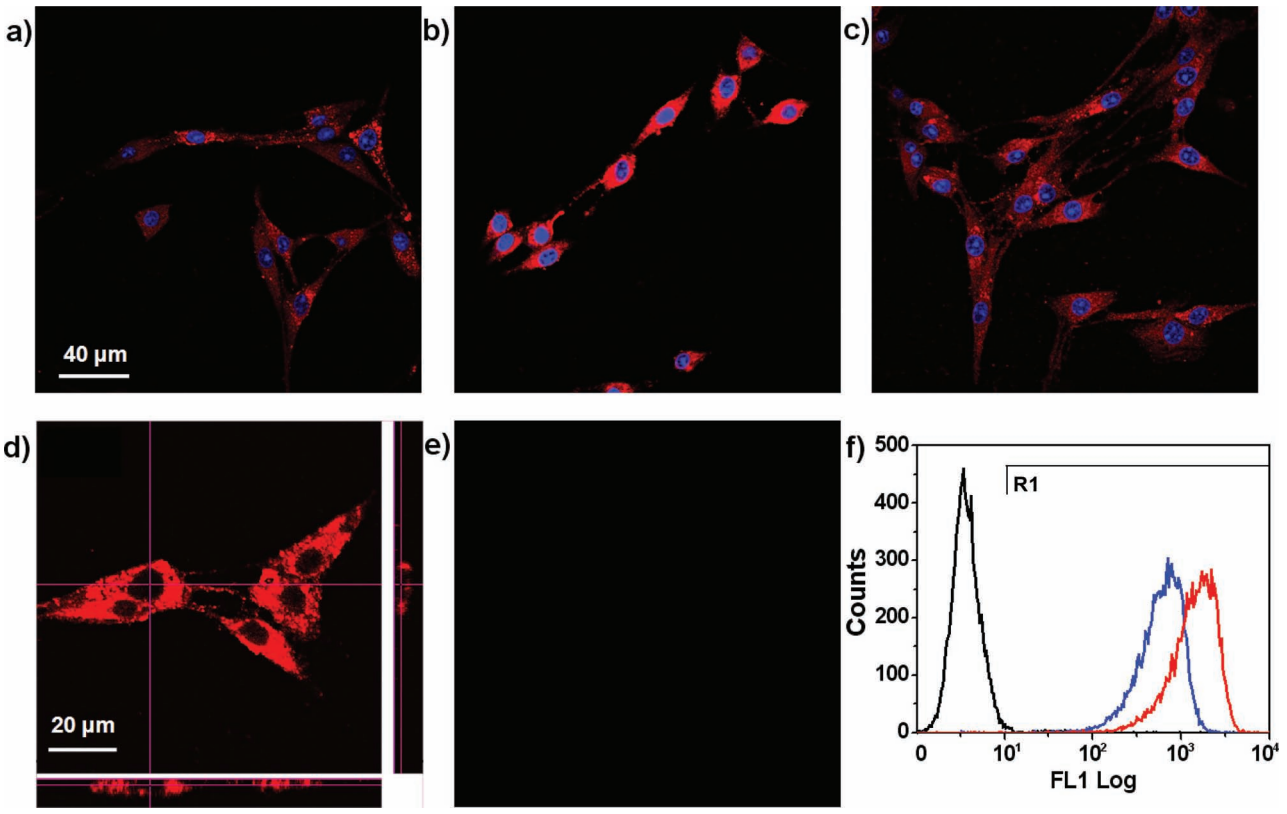

Figure 3. Confocal images of the MCF-7 breast cancer cells after 4 h incubation with the MCPNP (a) and FMCPNP (b) suspension at 0.25 mg/mL of NPs. c) Confocal image of the free folic acid-pretreated MCF-7 breast cancer cells after 4 h incubation with 0.25 mg/mL of FMCPNPs. The nuclei were stained by DAPI. d) 3D sectional confocal image of the MCF-7 breast cancer cells after 4 h incubation with 0.25 mg/mL of FMCPNPs. e) Confocal image of MCF-7 breast cancer cells without incubation with FMCPNPs. f) Flow cytometry histograms of pure MCF-7 cancer cells (black) and the cells after 4 h incubation with the MCPNP (blue) or FMCPNP (red) suspension at 0.25 mg/mL of NPs. Images (a,b,c,e) have the same scale bar.

72 h, respectively. The high cell viability (~100%) indicates that FMCPNPs have very low cytotoxicity during the tested period, which is beneficial to both in vitro and in vivo imaging.

2.3. In Vivo Fluorescence Imaging

To evaluate the capability of FMCPNPs as a dual-modal imaging agent for in vivo FR/NIR fluorescence and magnetic resonance imaging, the NPs were injected at a dosage of 7.84 mg Fe/kg and 2.48 mg PFVBT/kg into the mice via the tail vein. Murine hepatoma H22 tumor with overexpressed folate receptors was transplanted into the mice before the in vivo study.[18] **Figure 5**a shows the time-dependent excretion profile and tumor accumulation of FMCPNPs in murine hepatoma H22 tumor-bearing mice, using a Maestro EX in vivo fluorescence imaging system. The order of red, orange, yellow, green, and blue corresponds to the successive decrease in fluorescence intensity. Although the FMCPNPs are widely dispersed among the whole body of mouse at 1 h post-injection, they have a tendency to be enriched in the tumor tissue over time. The NP accumulation in tumor reaches a maximum at 6 h post-injection and clear tumor delineation is observed. The fluorescence intensity at the tumor site is 1182.7 ± 35.7 at 6 h post-injection, which is ~1.9 times of that at 1 h post-injection (617.8 ± 22.0). The specific in vivo tumor targeting ability of FMCPNPs is further evaluated on the same tumor-bearing mouse model using MCPNPs as a control. As displayed in Figure S5 in the Supporting Information, much higher fluorescence intensity is clearly observed at the tumor site of FMCPNP-treated mouse (1095.2 ± 26.5), which is twice brighter as compared to that of MCPNP-treated mouse (563.3 ± 30.8) at 6 h post-injection. These results suggest that the FMCPNPs are able to preferentially accumulate in tumor tissues not only through passive targeting resulted

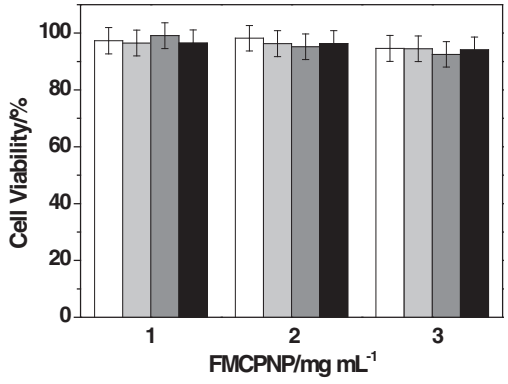

Figure 4. Metabolic viability of MCF-7 cells (white for 48 h and light gray for 72 h) and NIH/3T3 cells (gray for 48 h and black for 72 h) after incubation with FMCPNPs at different concentrations.

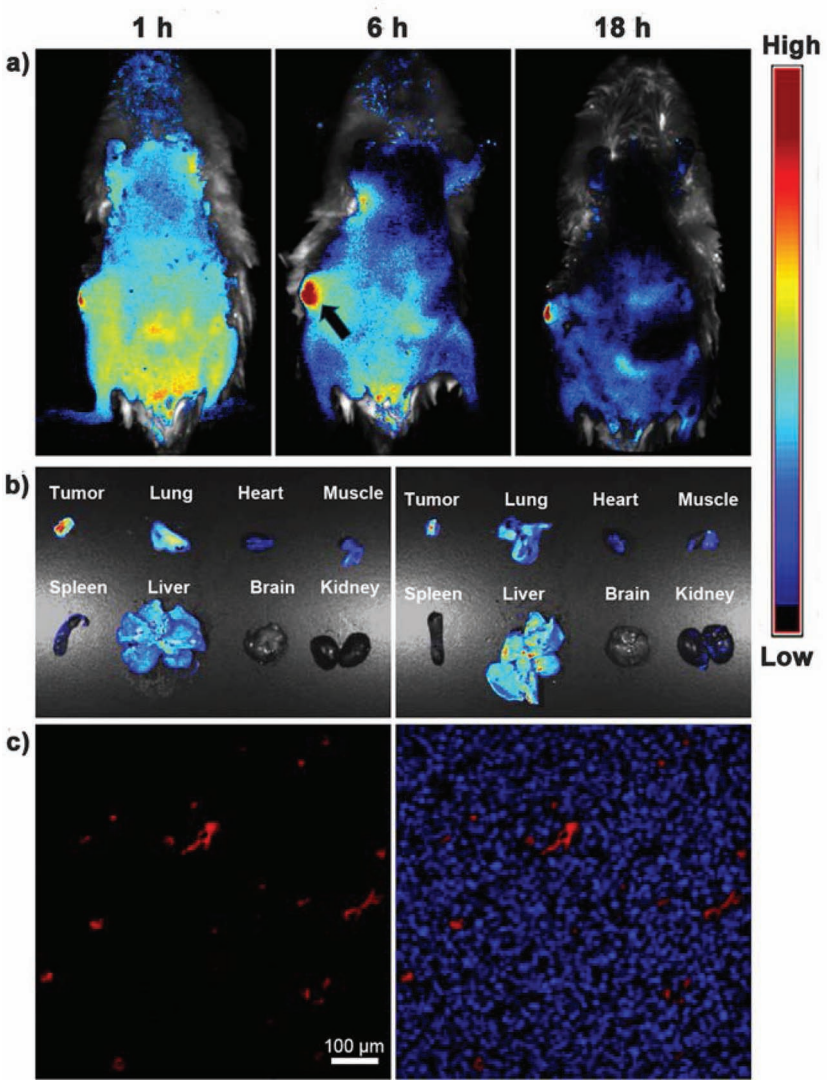

Figure 5. a) Representative in vivo fluorescence images of mouse injected with FMCPNPs acquired at 1 h, 6 h and 18 h post-injection. b) Fluorescence images of various organs from the mice treated with FMCPNPs (left) and MCPNPs (right), respectively at 12 h post-injection. c) Confocal images of sectioned tumor tissue harvested at 6 h post-injection. Left image shows the fluorescence of FMCPNPs in tumor section and right image shows the same image merged with 4′,6-diamidino-2-phenylindole stained nuclei (blue).

from the enhanced permeability and retention (EPR) effect due to their proper particle size (~180 nm) but also via folate receptor-mediated active targeting effect.[19] Since NPs in blood circulation generally enter the tumor via the leaky blood vessels,[20] the FMCPNPs tend to preferentially light up the most vascularized region of the tumor (tumor periphery region) at 1 h post-injection. As the time elapses, the fluorescence intensity in the majority of organs greatly decreases. However, the tumor tissue especially its periphery region is still clearly distinguishable at 18 h post-injection (707.5 ± 29.7). This result reveals that most of the FMCPNPs can be readily excreted from the body after primary imaging, implying good biocompatibility of the imaging agent.

The mice treated with FMCPNPs and MCPNPs were sacrificed at 12 h post-administration and various organs including liver, heart, lung, brain, spleen, kidney, muscle and tumor were isolated and imaged, respectively. As shown in Figure 5b, for the mice treated with FMCPNPs, a higher fluorescent signal is observed in the tumor as compared to that from other organs including liver. On the contrary, the fluorescence from tumor harvested from MCPNP-administrated mice shows no obvious difference as compared to that from liver, which further confirms the importance of folic acid functionalization for targeted tumor imaging. To confirm the accumulation of FMCPNPs in tumor, one mouse was sacrificed at 6 h post-injection and the tumor tissue was sectioned and imaged by confocal laser scanning microscopy. As shown in Figure 5c, some intense red fluorescent spots are clearly observed in the tumor slice, verifying the prominent uptake of FMCPNPs in the tumor at 6 h. An enlarged fluorescence image of Figure 5c (Figure S6 in the Supporting Information) shows that although many FMCPNPs are found in the interstitial area, some NPs are distributed in the tumor cells. Similarly, some fluorescence signal can also be distinguished from the tumor slice of mice treated with MCPNPs (Figure S7 in the Supporting Information). On the contrary, no autofluorescence from the tumor slice itself can be detected under the same imaging conditions (Figure S8 in the Supporting Information). As a result, FMCPNPs can serve as a FR/NIR fluorescent probe for tumor tissue imaging as well.

To further verify the targeting ability of FMCPNPs in in vivo studies, the mice were sacrificed to collect tumor tissues at 6 h post intravenous injection of 4 mg of FMCPNPs and MCPNPs, respectively. Quantitative studies using ICP-MS suggest that the concentrations of iron in tumor tissues from the mice administrated with FMCPNPs and MCPNPs are 35.5 ± 2.0 μg/g tumor and 20.2 ± 1.5 μg/g tumor at 6 h post-injection, respectively. As a result, the iron content per gram of tumor from the mice treated with FMCPNPs is ~1.76 times of that treated with MCPNPs at 6 h post-injection, which is consistent with the fluorescence quantification from Figure S5 (Supporting Information). Considering the encapsulation efficiencies of iron oxide in both FMCPNPs and MCPNPs are similar, the statistically higher iron concentration in tumors upon injection of FMCPNPs at 6 h as compared to that upon injection of MCPNPs ($P < 0.05$, $n = 3$) suggests that more FMCPNPs were accumulated in tumor tissues. Moreover, free folic acid competition experiments were further performed to directly evaluate the active targeting effect of FMCPNPs.[21] Upon folate receptor blocking by intravenous injection of free folic acid (200 μg) 15 min before the administration of FMCPNPs (4 mg), the concentration of iron in collected tumor tissues drops to

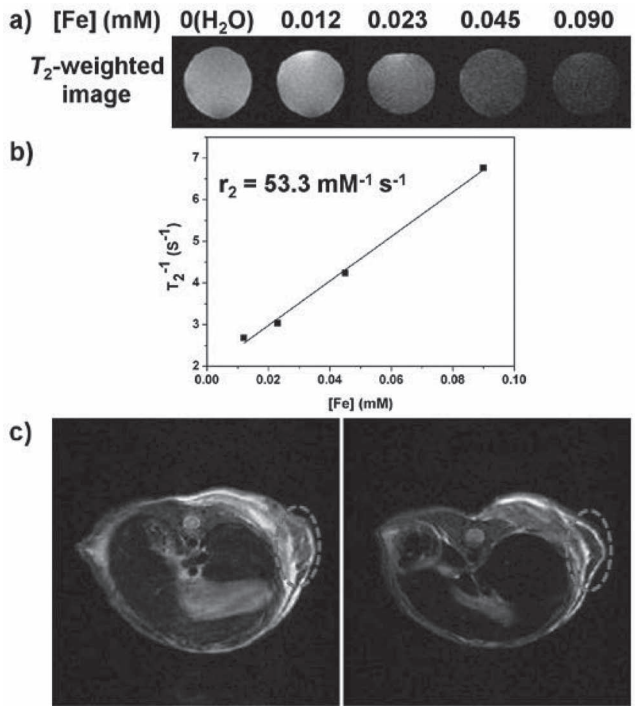

Figure 6. a) T_2-weighted MR images of FMCPNPs in water. b) T_2 relaxivity plot of aqueous suspension of FMCPNPs. c) Representative in vivo MR images of mouse pre-injection (left) and post-injection with FMCPNPs for 5 h (right).

23.9 ± 1.4 μg/g tumor at 6 h post-injection of FMCPNPs. Moreover, the sectioned tumor tissue from a free folic acid-pretreated mouse at 6 h post-injection of FMCPNPs was imaged by confocal laser scanning microscopy, showing some red fluorescent spots that indicate the accumulation of FMCPNPs (Figure S9 in the Supporting Information). These results indicate that both EPR effect and folate receptor-mediated active targeting effect are involved in the accumulation of FMCPNPs in the tumor tissue in vivo, which is superior to MCPNPs.

2.4. In Vivo Magnetic Resonance Imaging

The spin-spin relaxation times (T_2) of the FMCPNPs were investigated using a 7.0-T MRI instrument to demonstrate their utility in MRI. **Figure 6**a shows the T_2-weighted MRI of NP suspensions at various concentrations of Fe. The signal intensity of MR image decreases with increased concentration of FMCPNPs, indicating that the NPs can shorten the spin-spin relaxation time. The net effectiveness is expressed as T_2 relaxivity (r_2), which represents the reciprocal of the relaxation time per unit concentration.[22] As shown in Figure 6b, the FMCPNPs have a r_2 value of 53.3 mM^{-1} s^{-1}. In vivo MRI was conducted using the same mice intravenously injected with FMCPNPs for fluorescence imaging. Figure 6c shows the T_2-weighted MR images at 7.0 T before and after the NPs injection. At 5 h post-injection, an obvious drop in the MR signal is observed at the tumor site, indicating the prominent tumor uptake of NPs, which is in good accordance with the fluorescence imaging study. These studies verify that the FMCPNPs can serve as a promising dual-modal probe for simultaneous FR/NIR fluorescence and magnetic resonance imaging, which allows precise detection of the location and distribution of tumors in a living body.

3. Conclusions

In summary, we report the fabrication of dual-modal fluorescent-magnetic NPs with folate receptor-overexpressed cancer cell targeting ability by co-encapsulation of conjugated polymer and lipid-coated IOs into a mixture of PLGA-PEG-FOL and PLGA. The emission of the conjugated polymer is designed to fall into FR/NIR spectral window. Incorporation of lipid-coated IOs into these NPs yielded probes having superparamagnetic properties without sacrificing their fluorescence. To the best of our knowledge, it is the first time that conjugated polymer based NPs have been applied for in vivo FR/NIR fluorescence and magnetic resonance imaging. As a result, this work provides new opportunities to design conjugated polymer based multimodal platform through incorporating various reagents of specific functionalities (e.g., therapeutic drugs and Si-RNA), which holds great promises for various in vivo bioimaging and therapy applications in the near future.

4. Experimental Section

Materials: Poly[9,9-bis(2-(2-(2-methoxyethoxy)ethoxy)ethyl) fluorenyldivinylene] (PFV), poly[9,9-bis(2-(2-(2-methoxyethoxy)ethoxy)ethyl) fluorene-*alt*-4,7-(2,1,3-benzothiadiazole)] (PFBT), 9,9-bis(6′-bromohexyl)-2,7-divinylfluorene, 4,7-dibromobenzothiadiazole and oleic acid coated superparamagnetic iron oxide particles (OA-IOs) were synthesized according to literature.[23] Poly(DL-lactide-co-glycolide) (PLGA-COOH) (L:G molar ratio: 50:50, M_w: 44 000) was a gift from PURAC Asia Pacific, Singapore. Amine-poly (ethylene glycol)-amine (PEG bisamine, M_w: 2000) was purchased from Laysan Bio, Inc. PLGA-PEG-FOL was synthesized according to literature.[24] 1,2-Distearoyl-*sn*-glycero-3-phosphoethanolamine (DSPE), ethanol, dimethylformamide (DMF), triethylamine, dimethyl sulfoxide (DMSO), *N*-hydroxysuccinimide, 3-(4,5-dimethylthiazol-2-yl)-2,5-diphenyl tetrazolium bromide (MTT), dicyclohexylcarbodiimide, penicillin-streptomycin solution were purchased from Sigma-Aldrich. Fetal bovine serum (FBS) and trypsin-EDTA solution were purchased from Gibco (Lige Technologies, Ag, Switzerland). Tetrahydrofuran (THF) and dichloromethane (DCM) were obtained from Merck (Germany). Milli-Q water was supplied by Milli-Q Plus System (Millipore Corporation, Breford, USA). MCF-7 breast cancer cells and NIH/3T3 fibroblast cells were provided by American Type Culture Collection. Murine hepatic carcinoma cell line H22 was purchased from Shanghai Institute of Cell Biology (Shanghai, China). Male ICR mice (6-8 weeks old) were purchased from Animal Center of Drum-Tower Hospital (Nanjing, China).

Surface Coating of OA-IOs: OA-IOs (5 mg of IOs) were dispersed in 5 mL of water and mixed with 10 mL of methanol containing 40 mg of DSPE. The solution was mixed overnight to allow DSPE to encapsulate OA-IOs into a hydrophobic shell. The mixture was washed twice with methanol through centrifugation to remove the excess DSPE molecules. The obtained DSPE coated particles (DSPE-IOs) were dispersed in 5 mL of methanol to yield an IO solution (1 mg/mL) for further use.

Synthesis of Poly[9,9-bis(6′-(N,N-dimethylamino)hexyl)fluorenyldivinylene-alt-4,7-(2,1,3,-benzothiadiazole)] (PFVBT): A Schlenk tube was charged with 9,9-bis(6′-bromohexyl)-2,7-divinylfluorene (100 mg, 0.212 mmol), 4,7-dibromobenzothiadiazole (62 mg, 0.212 mmol), $Pd(OAc)_2$ (2 mg, 9 μmol), and P(o-tolyl)$_3$ (15 mg, 49 μmol). The Schlenk

tube was subsequently sealed with a rubber septum and degassed with three vacuum-argon cycles to remove air. DMF (1.6 mL) and triethylamine (0.8 mL) was then added to the Schlenk tube and the mixture was frozen, evacuated, and thawed three times to remove air. The polymerization was carried out at 100 °C under vigorous stir for 12 h. The product was then filtered through 0.22 μm syringe driven filter and poured into diethyl ether. The precipitate was collected and washed with methanol and acetone. After drying under vacuum for 24 h, PFVBT (108 mg, 81%) was collected as red fibers. ^{1}H NMR (500 MHz, $CDCl_3$, δ ppm): 8.14 (br 4 H), 7.93-7.36 (m, 8 H), 2.30 (br, 4 H), 2.13 (s, 12 H), 2.00 (br, 4 H), 1.30 (br, 4 H), 1.12 (br, 8 H), 0.73 (br, 4 H). ^{13}C NMR (125 MHz, $CDCl_3$, δ ppm): 154.05, 151.68, 141.21, 136.71, 133.89, 129.43, 127.04, 126.43, 123.92, 121.25, 120.18, 59.77, 55.17, 45.41, 40.51, 29.98, 27.59, 27.17, 23.82. M_n = 9500, M_w/M_n = 2.1.

Synthesis of PFVBT and OA-IOs Loaded NPs: PFVBT and OA-IOs loaded NPs were fabricated by double emulsion solvent extraction technique. In brief, an aqueous solution of OA-IOs (1 mg of IOs) was emulsified into 5 mL of dichloromethane solution containing 1 mg of PFVBT, 5 mg of PLGA-PEG-FOL and 45 mg of PLGA to form water-in-oil emulsion using a probe sonicator (XL2000, Misonix Incorporated, NY, 20 W for 30 s) over an ice bath. The water-in-oil emulsion was further mixed with an aqueous solution of PVA (0.5% w/v), followed by sonicating at 18 W output for 90 s. The obtained water-in-oil-in-water emulsion was then stirred at room temperature overnight to evaporate dichloromethane. The formed NP suspension was washed with MilliQ water through centrifugation for three times before collecting the final product.

Synthesis of PFVBT and DSPE-IOs Loaded NPs: PFVBT and DSPE-IOs loaded NPs were synthesized through a modified nanoprecipitation method. A tetrahydrofuran solution (5 mL) containing DSPE-IOs (1mg of IOs), 1 mg of PFVBT, 5 mg of PLGA-PEG-FOL and 45 mg of PLGA was poured into 30 mL of aqueous solution containing 10% (w/v) d-alpha-tocopheryl poly(ethylene glycol) 1000 succinate (TPGS) as the emulsifier. The mixture was sonicated for 90 s at 18 W output using a microtip probe sonicator. The emulsion was mixed with additional 100 mL of water and the mixture was stirred overnight in fumehood to evaporate tetrahydrofuran. The NP suspension was washed with MilliQ water through centrifuging for three times to collect the final product. PFVBT loaded NPs without IOs were also prepared following the same procedure.

Synthesis of Dual-Modal NPs: Dual-modal NPs (FMCPNPs) were synthesized through a modified nanoprecipitation method. In brief, a tetrahydrofuran solution (5 mL) containing PFVBT (1 mg), DSPE-IOs (4 mg of IOs), 5 mg of PLGA-PEG-FOL and 45 mg of PLGA was poured into 30 mL of aqueous solution containing 10% (w/v) d-alpha-tocopheryl poly(ethylene glycol) 1000 succinate (TPGS) as the emulsifier. The mixture was sonicated for 90 s at 18 W output using a microtip probe sonicator (XL2000, Misonix Incorporated, NY). The emulsion was mixed with additional 100 mL of water and the mixture was stirred overnight in fumehood to evaporate tetrahydrofuran. The NP suspension was washed with MilliQ water through centrifuging for three times to collect the final product.

ICP-MS Analysis: The fluorescent-magnetic NPs (1 mg) were added into 1 mL of concentrated nitric acid. The solution was then heated to 80 °C for 30 min to completely dissolve the NPs. The obtained solution was further diluted to 32 mL by MilliQ water and the samples were analyzed using inductively coupled plasma mass spectrometry (Agilent ICP-MS 7500 Series). The Fe content for each sample was calculated using a standard curve with ICP-MS standard.

Characterization: The UV-vis absorption spectra of NP suspensions were collected on a Shimadzu UV-1700 spectrophotometer. The fluorescence spectra of NP aqueous suspensions were measured using a fluorometer (LS-55, Perkin Elmer, USA) with an excitation wavelength of 518 nm. The average particle size of the NPs was determined by laser light scattering (LLS) with particle size analyzer (90 Plus, Brookhaven Instruments Co. USA) at a fixed angle of 90° at room temperature. The superparamagnetic properties of FMCPNPs were investigated by vibrating sample magnetometer (VSM, ADE magnetics EV-7, USA). The morphology of FMCPNPs was investigated by field emission scanning electron microscopy (FESEM, JSM-6700F, JEOL, Japan) and high-resolution transmission electron microscope (HR-TEM, JEM-2010F, JEOL, Japan). The surface chemistry of FMCPNPs was studied by X-ray photoelectron spectroscopy (XPS, AXIS His-165 Ultra, Kratos Analytical, Shimadzu Corporation, Japan). The fixed transmission mode was utilized with pass energy of 80 eV and the binding energy spectrum was recorded from 0 to 1100 eV.

The Influence of IO Surface Coating on the Optical Properties of Fluorescent-Magnetic Probes: In addition to PFVBT, another two conjugated polymers with different fluorescent colors were used to demonstrate the generality of the strategy, which are poly[9,9-bis(2-(2-(2-methoxyethoxy) ethoxy)ethyl) fluorenyldivinylene] (PFV, green) and poly[9,9-bis(2-(2-(2-methoxyethoxy)ethoxy)ethyl)fluorene-*alt*-4,7-(2,1,3-benzothiadiazol)] (PFBT, yellow). The chemical structures of PFV and PFBT are shown in Figure S10 in the Supporting Information. At the same polymer concentration, the fluorescence intensities of PFV and PFBT NPs co-encapsulated with OA-IOs are greatly decreased as compared to that with DSPE-IOs, respectively (Figure S10 in the Supporting Information). On the other hand, the fluorescence intensities of PFV and PFBT NPs co-encapsulated with DSPE-IOs are only slightly lower than that of the pure PFV and PFBT NPs, respectively.

Determination of PFVBT Encapsulation Efficiency: The encapsulation efficiency of PFVBT is defined as the ratio of PFVBT successfully encapsulated in FMCPNPs or MCPNPs to the total amount of PFVBT used in NP synthesis. The fluorescence intensity of a series of PFVBT solutions in THF at 612 nm was measured upon excitation at 518 nm to yield a standard curve of PFVBT fluorescence intensity versus concentration. Freeze-dried NPs (0.5 mg) were then dissolved in 1 mL of THF, 10 μL of which was further diluted into 1 mL of THF and the fluorescence intensity at 612 nm was obtained upon excitation at 518 nm. The amount of PFVBT encapsulated in 0.5 mg of NPs was then determined from the standard curve, and the encapsulation efficiency was further calculated.

Cell Cultures: MCF-7 breast cancer cells and NIH/3T3 fibroblast cells were cultured (37 °C, 5% CO_2) in RPMI 1640 medium containing 10% fetal bovine serum and 1% penicillin streptomycin. Before experiment, the cells were pre-cultured until confluence was reached.

Cytotoxicity of FMCPNPs: Methylthiazolyldiphenyl-tetrazolium (MTT) assays were used to assess the metabolic activity of MCF-7 breast cancer cells to study the cytotoxicity of FMCPNPs. MCF-7 cells were seeded in 96-well plates (Costar, IL, USA) at 4×10^4 cells/mL. After 24 h incubation, the medium was replaced by the FMCPNP suspension at a NP concentration of 1, 2 and 3 mg/mL, and the cells were then incubated for 48 and 72 h, respectively. After the designated time intervals, the wells were washed twice with 1× PBS buffer and 100 μL of freshly prepared MTT (0.5 mg/mL) solution in culture medium was added into each well. The MTT medium solution was carefully removed after 3 h incubation in the incubator at 37 °C. DMSO (100 μL) was then added into each well and the plate was gently shaken to dissolve all the precipitates formed. The absorbance of MTT at 570 nm was monitored by the microplate reader (Genios Tecan) after subtracting the absorbance of the corresponding control wells incubated with FMCPNPs at the same concentration but without the addition of MTT to eliminate the absorbance interference from PFVBT. Cell viability was expressed by the ratio of absorbance of the cells incubated with NP suspension to that of the cells incubated with culture medium only.

In Vitro Cellular Imaging: MCF-7 breast cancer cells were cultured in the confocal imaging chambers (LAB-TEK, Chambered Coverglass System) at 37 °C. After 80% confluence, the medium was removed and the adherent cells were washed twice with 1× PBS buffer. The FMCPNPs and MCPNPs in FBS-free RPMI 1640 medium at 0.25 mg/mL of NPs were then added to the chambers, respectively. After incubation for 4 h, the cells were washed three times with 1× PBS buffer and then fixed with 75% ethanol for 20 min, which were further washed twice with 1× PBS buffer. The cell monolayer was imaged by confocal laser scanning microscope (CLSM, Zeiss LSM 410, Jena, Germany) with imaging software (Fluoview FV1000) under the same experimental condition. To study the competitive effects of free folic acid on the endocytosis of

FMCPNPs, FBS-free RPMI medium containing 50 μg/mL of free folic acid was firstly added to the chamber. After 30 min, the medium was replaced by medium containing 0.25 mg/mL of FMCPNPs and 50 μg/mL of free folic acid. After 4 h incubation at 37 °C, the cells were then fixed for confocal imaging.

Flow Cytometry Study: Three groups of MCF-7 cancer cells were precultured in culture flask to achieve desired confluence, respectively. One group was used as the control without treatment. For the rest two groups, the medium was discarded and 0.25 mg/mL of FMCPNPs or MCPNPs in FBS-free RPMI 1640 medium was added, followed by incubation for 4 h at 37 °C, respectively. The control and sample groups were treated with 1× trypsin and washed with DMEM medium through centrifugation. The cell density was measured using a hemocytometer. Approximately 5×10^5 of MCF-7 cancer cells were dispersed in 2 mL of DMEM medium for both control and sample groups. Flow cytometry measurements were conducted using Cyan-LX (DakoCytomation). The mean fluorescence was determined by counting 10,000 events (λ_{ex} = 488 nm, 680/40 nm bandpass filter).

In Vivo Fuorescence and Magnetic Resonance Imaging: All animal experiments were performed in compliance with guidelines set by the Animal Care Committee at Drum-Tower Hospital. Male ICR mice implanted with murine hepatic carcinoma cell line H22 were used to investigate the fluorescence and MR imaging of the FMCPNPs. H22 tumor cells ($5\text{-}6 \times 10^6$ cells per mouse) were inoculated subcutaneously to the ICR mice at the right waist. H22 tumor-bearing mice were intravenously injected with 4 mg of FMCPNPs (7.84 mg Fe/kg and 2.48 mg PFVBT/kg) when the tumor volume reached a mean size of about 300 mm^3. For in vivo fluorescence imaging, the mice were anesthetized and placed on an animal plate heated to 37 °C. The time-dependent biodistribution in mice was imaged using the Maestro in vivo fluorescence imaging system (CRi Inc.). Light with a central wavelength at 523 nm was selected as the excitation source. In vivo spectral imaging from 560 to 800 nm at 10 nm steps was conducted with an exposure time of 150 ms for each image frame. Autofluorescence was removed by using spectral unmixing software. Scans were carried out at 1 h, 6 h, and 18 h post-injection. To assess the specific in vivo tumor targeting ability of FMCPNPs, H22 tumor-bearing mice were intravenously injected with 4 mg of FMCPNPs and MCPNPs, respectively, which were then imaged using the Maestro in vivo fluorescence imaging system. The imaging processes followed the same procedures. Scans were conducted at 1 h, 6 h, and 12 h post-injection. After 12 h post-administration, the mice were sacrificed and the tissues including liver, heart, lung, brain, spleen, kidney, muscle and tumor were harvested for isolated organ imaging. After 6 h post-injection, one mouse was sacrificed and the tumor tissue was resected and fixed in 4% paraformaldehyde for 2 h. And then the tumor was incubated in 20% sucrose/PBS overnight, embedded in Optimal Cutting Temperature (OCT) compound (Tissue-Tek) and cut into thin sections (6 μm) with a microtomy at −24 °C (Leica CM 1900 Rapid Sectioning Cryostat). After stained by DAPI, the tumor section was imaged by confocal laser scanning microscopy. For in vivo MR imaging, the sedated mice were scanned using a 7.0 T Micro-MR scanner (PharmaScan 70/17, Brucker) at 0 h, 5 h post-injection. Coronal and transversal cross section images were acquired for each mouse.

Quantification of Iron Contents in Tumor Tissues: H22 tumor-bearing mice with similar tumor sizes were randomly assigned to two groups (n = 3 mice per group, tumor weights are 123 ± 15 mg for FMCPNP-treated and 130 ± 12 mg for MCPNP-treated mice, respectively). FMCPNPs and MCPNPs (4 mg in 0.2 mL) were intravenously injected into the mice (n = 3 mice per group), respectively. At 6 h post-injection, the mice were sacrificed (n = 3 per group) and the tumor tissues were collected, weighed and completely decomposed on heating in concentrated nitric acid. After evaporation to dryness, the samples were dissolved in 2 N nitric acid solution for ICP-MS analysis. The contents of iron accumulated in tumor tissues were then determined from the standard curve with ICP-MS standard. The data were then normalized to the tissue weight.

Free Folic Acid Competition Experiments: In the free folic acid competition experiments, the mice were first injected with 200 μg of free folic acid (0.04 mL). After 15 min, 4 mg of FMCPNPs were intravenously injected into the mice. At 6 h post-injection, the mice were sacrificed (n = 3, average tumor weight of 135 ± 29 mg) and the tumor tissues were collected, weighed. The samples were processed according to the same procedure for quantification of iron contents in tumor with ICP-MS analysis.

Statistical Analysis: Quantitative data were expressed as mean ± SD. Statistical comparisons were made by ANOVA analysis and Student's *t*-test. *P* value < 0.05 was considered statistically significant.

Supporting Information

Supporting Information is available from the Wiley Online Library or from the author.

Acknowledgements

The authors are grateful to the National Research Foundation (R279-000-323-281), Temasek Defence Systems Institute (R279-000-305-232, R279-000-305-422 and R279-000-305-592), Institute of Materials Research and Engineering (IMRE/11-1C0213) and National Natural Science Foundation of China (No. 21074051) for financial support.

Received: September 20, 2011
Revised: March 26, 2012
Published online: April 30, 2012

[1] J. Gao, H. Gu, B. Xu, *Acc. Chem. Res.* **2009**, *42*, 1097.
[2] a) M. Liong, J. Lu, M. Kovochich, T. Xia, S. G. Ruehm, A. E. Nel, F. Tamanoi, J. L. Zink, *ACS Nano* **2008**, *2*, 889; b) C. Minelli, S. B. Lowe, M. M. Stevens, *Small* **2010**, *6*, 2336; c) A. Quarta, R. Di Corato, L. Manna, A. Ragusa, T. Pellegrino, *IEEE Trans. Nanobiosci.* **2007**, *6*, 298.
[3] a) D. K. Yi, S. T. Selvan, S. S. Lee, G. C. Papaefthymiou, D. Kundalita, J. Y. Ying, *J. Am. Chem. Soc.* **2005**, *127*, 4990; b) S. T. Selvan, P. K. Patra, C. Y. Ang, J. Y. Ying, *Angew. Chem. Int. Ed.* **2007**, *46*, 2448; c) J. H. Gao, H. W. Gu, B. Xu, *Acc. Chem. Res.* **2009**, *42*, 1097.
[4] a) Y. Lu, Y. Yin, B. T. Mayers, Y. Xia, *Nano Lett.* **2002**, *2*, 183; b) F. Bertorelle, C. Wilhelm, J. Roger, F. Gazeau, C. Menager, V. Cabuil, *Langmuir* **2006**, *22*, 5385; c) J. Y. Kim, J. E. Lee, S. H. Lee, J. H. Yu, J. H. Lee, T. G. Park, T. H. Hyeon, *Adv. Mater.* **2008**, *20*, 478.
[5] A. M. Smith, H. Duan, A. M. Mohs, S. Nie, *Adv. Drug Delivery Rev.* **2008**, *60*, 1226.
[6] a) Y. He, Z. H. Kang, Q. S. Li, C. H. A. Tsang, C. H. Fan, S. T. Lee, *Angew. Chem. Int. Ed.* **2009**, *48*, 128; b) Y. He, Y. Y. Su, X. B. Yang, Z. H. Kang, T. T. Xu, R. Q. Zhang, C. H. Fan, S. T. Lee, *J. Am. Chem. Soc.* **2009**, *131*, 4434.
[7] a) T. Mokari, E. Rothenberg, I. Popov, R. Costi, U. Banin, *Science* **2004**, *304*, 1787; b) H. S. Hu, X. H. Gao, *J. Am. Chem. Soc.* **2010**, *132*, 7234.
[8] D. T. McQuade, A. E. Pullen, T. M. Swager, *Chem. Rev.* **2000**, *100*, 2537.
[9] a) F. Feng, F. He, L. L. An, S. Wang, Y. L. Li, D. B. Zhu, *Adv. Mater.* **2008**, *20*, 2959; b) H. Jiang, P. Taranekar, J. R. Reynolds, K. S. Schanze, *Angew. Chem. Int. Ed.* **2009**, *48*, 4300; c) K. Li, B. Liu, *Polym. Chem.* **2010**, *1*, 252.
[10] a) J. H. Moon, W. McDaniel, P. MacLean, L. F. Hancock, *Angew. Chem. Int. Ed.* **2007**, *46*, 8223; b) C. Wu, B. Bull, C. Szymanski, K. Christensen, J. McNeil, *ACS Nano* **2008**, *2*, 2415; c) K. Li, J. Pan, S. S. Feng, A. W. Wu, K. Y. Pu, Y. T. Liu, B. Liu, *Adv. Funct. Mater.* **2009**, *19*, 3535; d) P. Howes, R. Thorogate, M. Green,

S. Jickells, B. Daniel, *Chem. Commun.* **2009**, 2490; e) X. Feng, Y. Tang, X. Duan, L. Liu, S. Wang, *J. Mater. Chem.* **2010**, *20*, 1312; f) P. Howes, M. Green, J. Levitt, K. Suhling, M. Hughes, *J. Am. Chem. Soc.* **2010**, *132*, 3989; g) K. Y. Pu, K. Li, J. B. Shi, B. Liu, *Chem. Mater.* **2009**, *21*, 3816; h) K. Y. Pu, K. Li, B. Liu, *Chem. Mater.* **2010**, *22*, 6736; i) K. Li, Y. T. Liu, K. Y. Pu, S. S. Feng, R. Y. Zhan, B. Liu, *Adv. Funct. Mater.* **2011**, *21*, 287.

[11] a) D. Tuncel, H. V. Demir, *Nanoscale* **2010**, *2*, 484; b) Z. Y. Tian, J. B. Yu, C. F. Wu, C. Szymanski, J. McNeill, *Nanoscale* **2010**, *2*, 1999.

[12] P. Howes, M. Green, A. Bowers, D. Parker, G. Varma, M. Kallumadil, M. Hughes, A. Warley, A. Brain, R. Botnar, *J. Am. Chem. Soc.* **2010**, *132*, 9833.

[13] J. V. Frangioni, *Curr. Opin. Chem. Biol.* **2003**, *7*, 626.

[14] K. Y. Pu, K. Li, B. Liu, *Adv. Funct. Mater.* **2010**, *20*, 2770.

[15] W. Wang, Y. Xu, D. I. C. Wang, Z. Li, *J. Am. Chem. Soc.* **2009**, *131*, 12892.

[16] a) S. H. Lee, Z. Zhang, S. S. Feng, *Biomaterials* **2007**, *28*, 2041; b) C. Prashant, M. Dipak, C. T. Yang, K. H. Chuang, J. Ding, S. S. Feng, *Biomaterials* **2010**, *31*, 5588.

[17] a) J. Sudimack, R. J. Lee, *Adv. Drug Delivery Rev.* **2000**, *41*, 147; b) V. Dixit, J. V. Bossche, D. M. Sherman, D. H. Thompson, R. P. Andres, *Bioconjugate Chem.* **2006**, *17*, 603.

[18] T. Lu, J. Sun, X. Chen, P. Zhang, X. Jing, *Macromol. Biosci.* **2009**, *9*, 1059.

[19] W. Zhang, Y. Shi, Y. Z. Chen, J. Ye, X. Y. Sha, X. L. Fang, *Biomaterials* **2011**, *32*, 2894.

[20] J. Xie, K. Chen, J. Huang, S. Lee, J. Wang, J. H. Gao, X. G. Li, X. Y. Chen, *Biomaterials* **2010**, *31*, 3016.

[21] I. A. Jammaz, B. Al-Otaibi, S. Amer, S. M. Okarvi, *Nucl. Med. Biol.* **2011**, *38*, 1019.

[22] H. Yang, Y. M. Zhuang, H. Hu, X. X. Du, C. X. Zhang, X. Y. Shi, H. X. Wu, S. P. Yang, *Adv. Funct. Mater.* **2010**, *20*, 1733.

[23] a) K. Y. Pu, B. Liu, *Adv. Funct. Mater.* **2009**, *19*, 277; b) K. Li, Y. T. Liu, K. Y. Pu, S. S. Feng, R. Y. Zhan, B. Liu, *Adv. Funct. Mater.* **2011**, *21*, 287; c) K. Y. Pu, L. Cai, B. Liu, *Macromolecules* **2009**, *42*, 5933; d) B. Liu, G. C. Bazan, *Proc. Natl. Acad. Sci. U.S.A.* **2005**, *102*, 589; e) W. Wang, Y. Xu, D. I. C. Wang, Z. Li, *J. Am. Chem. Soc.* **2009**, *131*, 12892.

[24] F. Esmaeili, M. H. Ghahremani, S. N. Ostad, F. Atyabi, M. Seyedabadi, M. R. Malekshahi, M. Amini, R. Dinarvand, *J. Drug Targeting* **2008**, *16*, 415.